Journal of Materials Chemistry B

Accepted Manuscript

ROYAL SOCIETY OF CHEMISTRY

www.rsc.org/materialsB

Journal Name

RSCPublishing

ARTICLE

Enzymatic Electrochemical Glucose Biosensors by Mesoporous 1D Hydroxyapatite on 2D Reduced Graphene Oxide

G. Bharath,[a] Rajesh Madhu,[b] Shen-Ming Chen,[b] Vediappan Veeramani,[b] A. Balamurugan,[a] D. Mangalaraj,[a] C. Viswanathan,[a] N. Ponpandian*,[a]

Cite this: DOI: 10.1039/x0xx00000x

Received 00th January 2014,
Accepted 00th January 2014

DOI: 10.1039/x0xx00000x

www.rsc.org/

A novel hydrothermal process was used for the preparation of hydroxyapatite (HAp) nanorods on two dimensional reduced graphene oxides (RGO). The hydrothermal reaction temperature improves the crystallinity of HAp and partially reduces the graphene oxide (GO) to RGO. The crystalline structure, chemical composition and morphology of the prepared nanocomposites were characterized by using various analytical techniques. Nanorods of HAp with a diameter and length of ~ 32 and 60-85 nm were grown on basal planes and edges of the layered RGO sheets. The estimated specific surface area and pore size distribution are 120 m^2g^{-1} and 5.6 nm respectively. We also report the direct electrochemistry of glucose oxidase (GOx) on 1D HAp on 2D RGO nanocomposite modified glassy carbon electrode (GCE) for glucose sensing. The electrocatalytic and electroanalytical applications of the proposed RGO/HAp/GOx modified GCE were studied by cyclic voltammetry (CV) and amperometry. The increased electron rate constant of 3.50 s^{-1} was obtained for the modified GCE. The reported biosensor exhibits a superior detection limit and higher sensitivity *ca.* 0.03 mM and 16.9 μA mM^{-1} cm^{-2} respectively, with a wide linear range of 0.1-11.5 mM. The tremendous analytical parameters of the reported sensor, surpassing the related modified electrodes, rendering practical industrial applications.

1. Introduction

Diabetes mellitus is a metabolic disorder which has been differentiated as insulin deficiency and hyperglycemia. It brings a severe complication to the human body, such as kidney failure, heart disease, strokes, and blindness, *etc*. However, still there are some difficulties in accurate determination and monitoring the glucose level based on the conventional techniques. Recently, the nanomaterial provides an accurate detection of glucose using several physical and chemical methods such as electrochemical, colorimetric and electro-chemiluminescence assay, *etc*. Among these, electrochemical detection is a significant technique for accurate sensitive detection of glucose.[1] Several reports were available for the detection of glucose using enzyme based modified electrodes. The glucose oxidase (GOx) is a most prevalent enzyme which has been used for high sensitive and specific detection of glucose by electrochemical method. GOx converts glucose to glucono-d-lactone following the reduction of flavin adenine dinucleotide (FAD) resulting the $FADH_2$. This $FADH_2$ reoxidized by dissolved O_2 producing hydrogen peroxide (H_2O_2). Further, the H_2O_2 is oxidized to O_2 when a working potential is applied to the biosensor. The electric current produced in the sensor is proportional to the glucose concentration. There are still some disadvantages of sensitive and selective determination of glucose by enzyme-based

[a]*Department of Nanoscience and Technology, Bharathiar University, Coimbatore 641 046, India.*
E-mail: ponpandian@buc.edu.in
[b]*Department of Chemical Engineering and Biotechnology, National Taipei University of Technology, Taipei 10608, Taiwan.*

electrochemical glucose biosensors. One of the reasons may be the deprived stability due to the inherent nature of enzymes.[2,3] Hence, it is appropriate to explore the highly stable enzymatic biosensor by suitably modify/replace with present new materials. Graphene based carbon nanomaterials offers the probability to efficiently adsorbed GOx on their surface to improve sensitivity, selectivity and response speed of the biosensors.[2-5] These materials have widespread applications due to their size, shape and superior optical, mechanical, electronic, electrochemical and magnetic properties due to their high specific surface area (SSA).[6] The increased SSA of composite provide a better matrix for the immobilization of GOx, and then enables larger amounts of GOx to immobilize on the surfaces and basal planes of graphene sheets. The surfaces of the graphene has various oxygenated groups such as carbonyl and carboxyl groups located at the edges and more number of the hydroxyl and epoxy group at the basal plane which was produced during the oxidation of graphite. These oxygenated functional groups can offer plenty of reaction sites for anchoring the external organic species, such as small molecules, biomacromolecules, DNA, several protein and inorganic nanoparticles without using any cross-linking substances. The major drawbacks of the graphene is their poor dispersion capability in aqueous solution due to the strong hydrophobicity on the large SSA of a carbon monolayer cause to extremely hard and easily restacking, particularly for use in biological organisms and adsorption of biomolecules. Meanwhile, the incorporation of nanoparticles on graphene prevents the aggregation of individual graphene nanosheets due to the strong Van der Waals interaction. In addition, the functional groups of graphene can promote nucleation sites for the growth of nanoscaled hydroxyapatite (HAp), CuO nanoflowers, WO_3 nanowire, and noble metals (Au, Pd and Pt), and various transition elements for diverse applications.[12-14] Recent investigation on nanocomposites of metal oxides and ceramics significantly improves the electrochemical biosensing.[15] Instead of biomolecules adsorption, the hydroxyapatite ($Ca_{10}(PO_4)_6(OH)_2$, HAp) nanostructures have become a topic of extreme interest due to their distinctive affinity to biomolecules with a large adsorption capacity for separating biomolecules such as proteins, DNA, *etc*. The physical and chemical properties of HAp strongly depend on their crystallinity, dimensional anisotropy and morphology of the HAp for essential constructive applications. The geometrical structures of HAp play an important role in adsorbed biomolecules through electrostatic attractions. The crystal structure of HAp includes Ca^{2+}, PO_4^{3-} and OH^- ions. The positively charged Ca^{2+} sites surrounded by negatively charged tetrahedral PO_4^{3-} units and OH^- ions occupy columns parallel to the hexagonal axis. The Ca^{2+} ions are mainly present at *a (b)*-planes and PO_4^{3-} and OH^- ions are present in the *c*-planes.[16,17] These Ca^{2+} and PO_4^{3-} are responsible for the adsorption on its surfaces. Nanostructures of HAp were already prepared with different morphologies such as nanotubes, nanorods, nanowires and sphere. Among these, HAp nanorods exhibit small dimensions, well crystalline and high surface area with excellent adsorption capacity.[16] Also, the HAp combined with carbon provides an excellent mechanical and electrochemical sensing behavior.[17-18] Recently, hydroxyapatite were successfully grown on reduced graphene oxide sheets using simple co-precipitation technique.[19] Also, the hydroxyapatite was deposited on pristine and chitosan functionalized graphene oxide sheets by bio mineralization process. These bionanocomposites are promising materials to enhance the mechanical properties and *in-vitro* bioactivity.[20] The graphene/metal oxides, graphene/conducting polymer, hydroxyapatite/Nafion nanocomposite were systematically explored for electrochemical biosensors and used to determine the H_2O_2, glucose, dopamine, ascorbic acid and uric acid.[2-5,19] These attractive electrochemical properties of RGO/HAp nanocomposite could provide improved electron transfer between glucose oxidase (GOx) in the conducting electrodes for glucose sensing. Nevertheless, with an extensive literature survey, this is the first report for the 1D HAp grown on 2D RGO sheets prepared by hydrothermal technique for enzymatic electrochemical glucose biosensors.

Herein, we report a novel strategy to synthesize 1D HAp grown on 2D RGO by using a simple hydrothermal process. This process improves the crystallinity by the re-crystallization process which promotes the formation of nanorods. Simultaneously, the GO reduces to form RGO and a possible formation mechanism has also been proposed. Further, a novel biosensor was fabricated by immobilization of GOx on a glassy carbon electrode (GCE) modified with prepared nanocomposite which exhibits the excessive biocompatibility toward glucose biosensor. The glucose determination has been

realized in mediator-free conditions. This biosensor demonstrates long time stability, high selectivity and appreciable reproducibility.

2. Experimental Section

2.1 Reagents and materials

Graphite flakes (~105 μm flakes), calcium chloride di-hydrate ($CaCl_2.\ 2H_2O$), di-ammonium hydrogen phosphate ($(NH_4)_2(HPO_4)$) were purchased from Sigma Aldrich. Potassium permanganate ($KMnO_4$), sodium nitrate ($NaNO_3$), sulfuric acid (H_2SO_4 98%), hydrogen peroxide (H_2O_2), ammonium hydroxide (NH_4OH) and ethanol were purchased from Himedia Laboratory, India. All the chemicals were of analytical grade and used without further purification.

2.2 Synthesis of HAp nanorods on reduced graphene oxide (RGO) nanosheets

Graphite oxide was synthesized by using modified Hummer's method.[21] The HAp nanorods on reduced graphene oxide (RGO) nanosheets were synthesized by simple hydrothermal technique. In a typical process, 30 mg of graphite oxide was dissolved in 30 ml of deionized water by ultrasonic dispersion for 30 min to form a stable brown colour graphene oxide (GO) solution. Later, 0.5 mM of calcium chloride ($CaCl_2.2H_2O$) was dissolved into the above homogeneous GO solution. Then, 0.3 mM of di-ammonium hydrogen phosphate ($(NH_4)_2(HPO_4)$) was dissolved in 30 ml of deionized water and gradually added to the above solution. The pH of the solution was adjusted between 10 and 10.5 by adding ammonium hydroxide solution (30%). Further, this mixed solution was transferred to a Teflon lined stainless steel autoclave with tightly sealed and placed in the hot air oven for hydrothermal treatment at 180^{o}C for 12h. Subsequently, the autoclave was slowly cooled to room temperature naturally. Finally the precipitate was washed with deionized water and ethanol several times to remove the excess ions in the suspension. The obtained final product was dried in vacuum oven at 70^{o}C for overnight before further characterization.

2.3 Characterization

The morphology and elemental analysis of the nanocomposites were studied by field emission scanning electron microscope (FEI Quanta–250 FEG). The structural properties of the samples were characterized by PANalytical (X'Pert-Pro) X-ray diffractometer with CuKα1 radiation. Raman scattering was performed in a JY-1058 Raman spectrometer. The functional groups of the composite were identified by Bruker Tensor 27 Fourier transform infrared spectrometer (FTIR). The absorbance spectra were recorded by JascoV-650 UV-Vis spectrophotometer. Surface area and pore size distribution was determined by using a micromeritics ASAP 2020 surface area analyzer.

2.5 Fabrication of RGO/HAp/GOx Modified Electrode

The surface of the GCE was carefully polished with mirror finish by using alumina in water slurry and washed with deionized water. It was further cleaned by ultrasonication with ethanol containing water for a few minutes before the surface modification of the electrode. The prepared RGO/HAp nanocomposite was dispersed in water (0.1g/ml) and sonicated for 2 h to obtain the stable dispersion. About 6 μl of RGO/HAp dispersion with optimized concentration was drop cast on the pre-cleaned GCE and dried in hot air oven at 30°C. The fresh GOx solution was prepared by using phosphate buffered saline (PBS) at pH 7 and stored in refrigerator when not in use. In order to immobilize GOx on the modified GCE with RGO/HAp nanocomposite, 8 μl of GOx with optimized concentration was drop cast and allowed to dry at room temperature. Finally, the RGO/HAp/GOx modified GCE was gently rinsed a few times with deionized water to remove the loosely bound GOx. The fabricated RGO/HAp/GOx electrode was used for further measurements and stored in 4ºC under dry condition when not in use.

3. Results and Discussions

3.1 Morphological and structural analysis

The surface morphology and microstructure of the samples were observed by using field emission scanning electron microscopy (FESEM) and transmission electron microscopy (TEM). As shown in Fig. 1a,b for the FESEM and TEM micrographs of reduced graphene oxide (RGO) sheets obtained by a simple hydrothermal treatment of graphene oxide (GO) at 180^{o}C for 12 hours. The obtained RGO demonstrates that an ultrathin flexible sheet-like and transparent wrinkled-like morphology. Fig. 1c-d shows the FESEM images for the RGO/HAp nancomposite with different magnifications for the

1D nanorods like HAp grown on 2D graphene oxide sheets. The average diameter and length of the HAp nanorods were ~ 32 and 60-85 nm respectively. The magnified images shown the agglomeration free HAp nanorods spread on the reduced graphene oxide sheets. Also, un-restacking of graphene subsequently supports and maintains their dynamic high surface area. This provides an increase in the available chemically reactive sites without agglomeration. The functional group of graphene oxide such as hydroxyl (-OH), carboxylic (-COOH), and epoxy groups can offer favored nucleation sites for the growth of HAp nanorods. It enables the growth of homogeneously well dispersed HAp nanorods on reduced graphene oxide sheets. The HAp nanorods are distributed on the surface of graphene oxide sheets through weekly bonded Van der Waals interaction. The higher magnification FESEM image in Fig. 1d (inset) clearly shows the individual morphology of HAp nanorods.

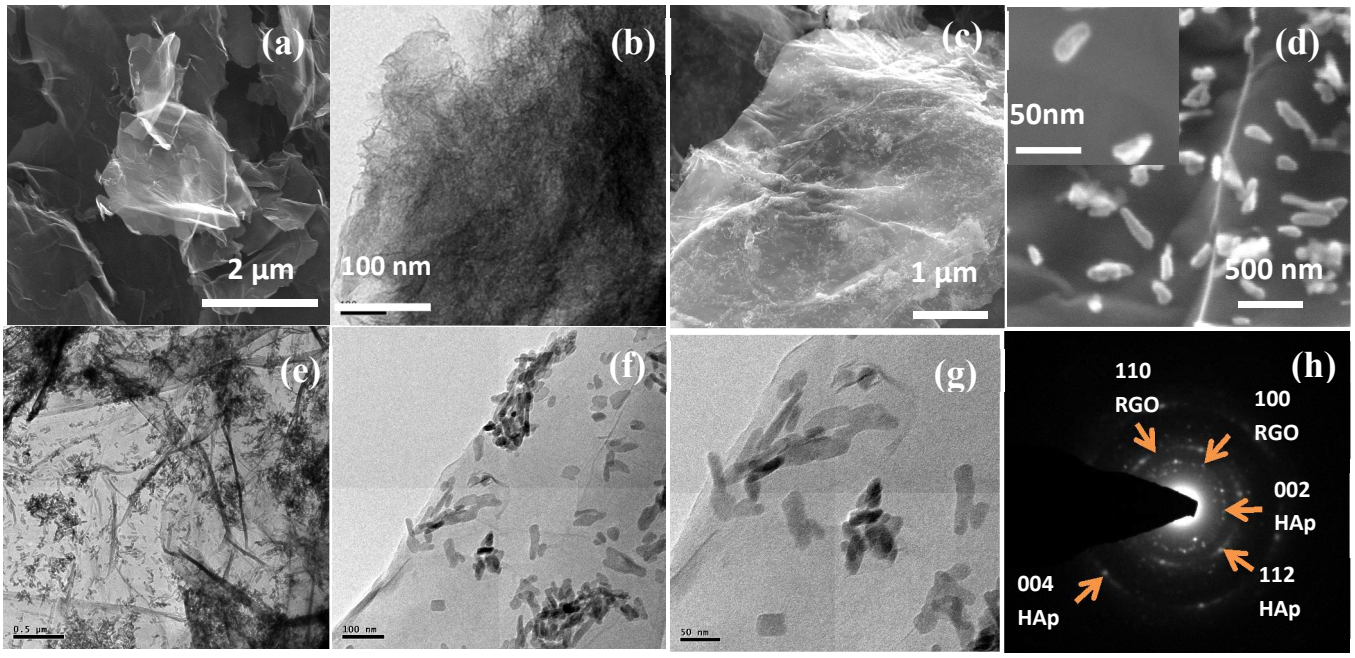

Fig. 1 (a,b) FESEM and TEM images for the highly reduced graphene oxide (RGO) sheets obtained by a simple hydrothermal treatment of graphene oxide (GO) at 180°C for 12 hours. (c,d) FESEM images for the RGO/HAp nanocomposite with different magnifications. TEM micrographs of the synthesized HAp/RGO nanocomposite with different magnification (e-g) and corresponding selected area electron diffraction (SAED) pattern (h).

The crystalline structure and morphology of the HAp/RGO nanocomposite was further investigated by transmission electron microscopy (TEM). Fig. 1 (e-g) shows low and high magnification TEM images of the HAp/RGO nanocomposite. The TEM images confirms the 1D like HAp nanorods were dispersed on 2D like reduced graphene oxide sheets by Van der Waals interaction. HAp nanorods have the average size of 60 to 85 nm in length and 32 nm in diameter. Fig. 1 (h) is the corresponding selected area electron diffraction (SAED) pattern for the HAp/RGO nanocomposite. The diffraction rings are very well indexed to faint six-fold symmetry and polycrystalline diffraction pattern of graphene and a polycrystalline diffraction pattern of hexagonal HAp phase.

The 1D on 2D structure without agglomeration of RGO/HAp nanocomposite shows higher specific surface area (SSA). The specific surface area (SSA) and pore size of the RGO/HAp nanocomposite was further validated by nitrogen physisorption (adsorption/desorption) isotherms. Fig. 2 shows the sorption isotherm corresponding to the Type-IV isotherm at a relative pressure (p/po) between 0.1 to 1 for the RGO/HAp nanocomposite.

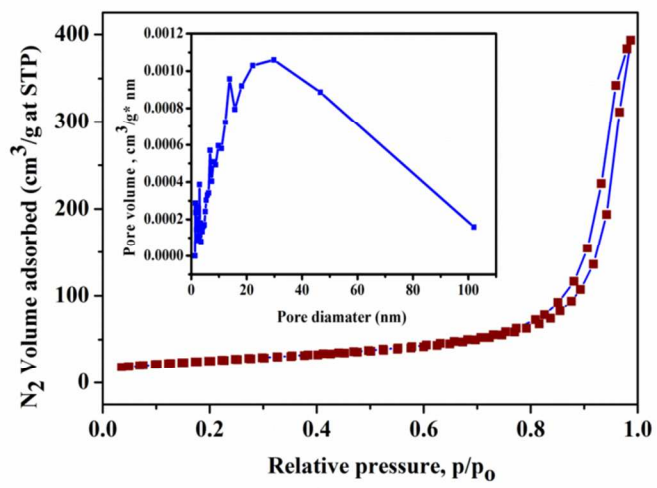

Fig. 2 Nitrogen-Adsorption/desorption isotherms and pore size distribution of RGO/HAp nanocomposite.

The SSA and the average pore size were calculated by Brunauer-Emmett-Teller (BET) method of adsorption analysis, and the average values were 120 m^2g^{-1} and 5.6 nm, respectively for the RGO/HAp nanocomposite. The phase formation and crystallanity of RGO and RGO/HAp nanocomposite were investigated by X-ray powder diffraction. Fig. 3a shows the diffraction pattern for the RGO, and a broad diffraction peak appeares at 25° corresponds to (002) plane and which confirms the short range order in the stacked graphene sheets and there was a significant reduction of GO to RGO under a hydrothermal reduction process. The strong diffraction peaks at 26.2, 32.1, 32.5, 33.2 and 34.3° corresponds to the hexagonal structured hydroxyapatite nanorods (JCPDS # 09-0432). The average crystallite sizes were estimated from the main peaks by using Scherrer formula and it was ~15 nm.

Furthermore, the order and disorder properties were studied by using Raman spectroscopy. Fig. 3b shows the room temperature Raman spectra for GO, HAp and RGO/HAp nanocomposite. The three major peaks at 1346, 1580 and 2714 cm^{-1} corresponds to the well-known D, G and 2D band of graphene oxide and RGO/HAp nanocomposite respectively. The D band at 1346 cm^{-1} was associated with the vibrations of A_{1g} symmetry of sp^3 carbon atoms and correlated to defect ordered structural peak. The G band arises due to the in plane vibration of the E_{2g} phonon of carbon sp^2 atoms. Also, the single intense second-order 2D band appears at 2714 $cm^{-1}$and it depends on the number of graphene layers present in the synthesized samples. As shown in Fig. 3b the peaks at 416, 574 and 1048 cm^{-1} were attributed to v_2 symmetrical bending vibration of PO_4^{3-}, v_3 asymmetrical stretching mode of PO_4^{3-} and v_4 anti-symmetric bending of PO_4^{3-} modes. The sharp peak at 947 cm^{-1} was assigned to the symmetric stretching v_1 (PO_4^{3-}) corresponding to free tetrahedral phosphate ions. Fig. 3c shows the Fourier transform infrared (FTIR) spectra for the as-prepared GO, HAp and RGO/HAp nanocomposite. In the pure HAp spectrum, intense peaks at 568 and 601 cm^{-1} were due to the bending vibrations of the O-P-O in the PO_4^{3-} groups. The asymmetric stretching vibrations of the P-O in the PO_4^{3-} groups were located at 1099 and 1037 cm^{-1}. The intense peaks at 3439 and 1637 cm^{-1} indicate the bending modes of H_2O. The characteristic peaks of the OH- stretching mode can be seen at 3574 and 632 cm^{-1}. The characteristic absorption peaks of methylene groups (CH_2), which were present due to the RGO/HAp nanocomposite was observed at 2853 and 2926 cm^{-1} as shown in Fig. 3c. The high resolution XPS spectrum was efficiently employed to analysis the structural composition of RGO/HAp nanocomposites as shown in Fig. 3d. As shown in Fig. 3d, the high resolution XPS spectrum of Ca2p exhibits two prominent peaks attributed at 347.5 and 350.4 eV, corresponding to the $Ca2p_{3/2}$ and $Ca2p_{1/2}$, respectively. The High resolution XPS spectrum exhibits at 133 eV cause to presence of phosphate group (P2p) in the HAp. The C1s contain nonoxygenated aromatic sp^2 carbon ring (C-C) at 284.5 eV and oxygenated functional group of carbon sp^2 C-O attributed at 286.29 eV. The O1s spectra shows two intense peaks at 529.84 and 531.84 eV, associated may be the anionic oxygen in hydroxyl (OH) and residual oxygen functional groups are present in the RGO sheets.

Journal Name RSCPublishing

ARTICLE

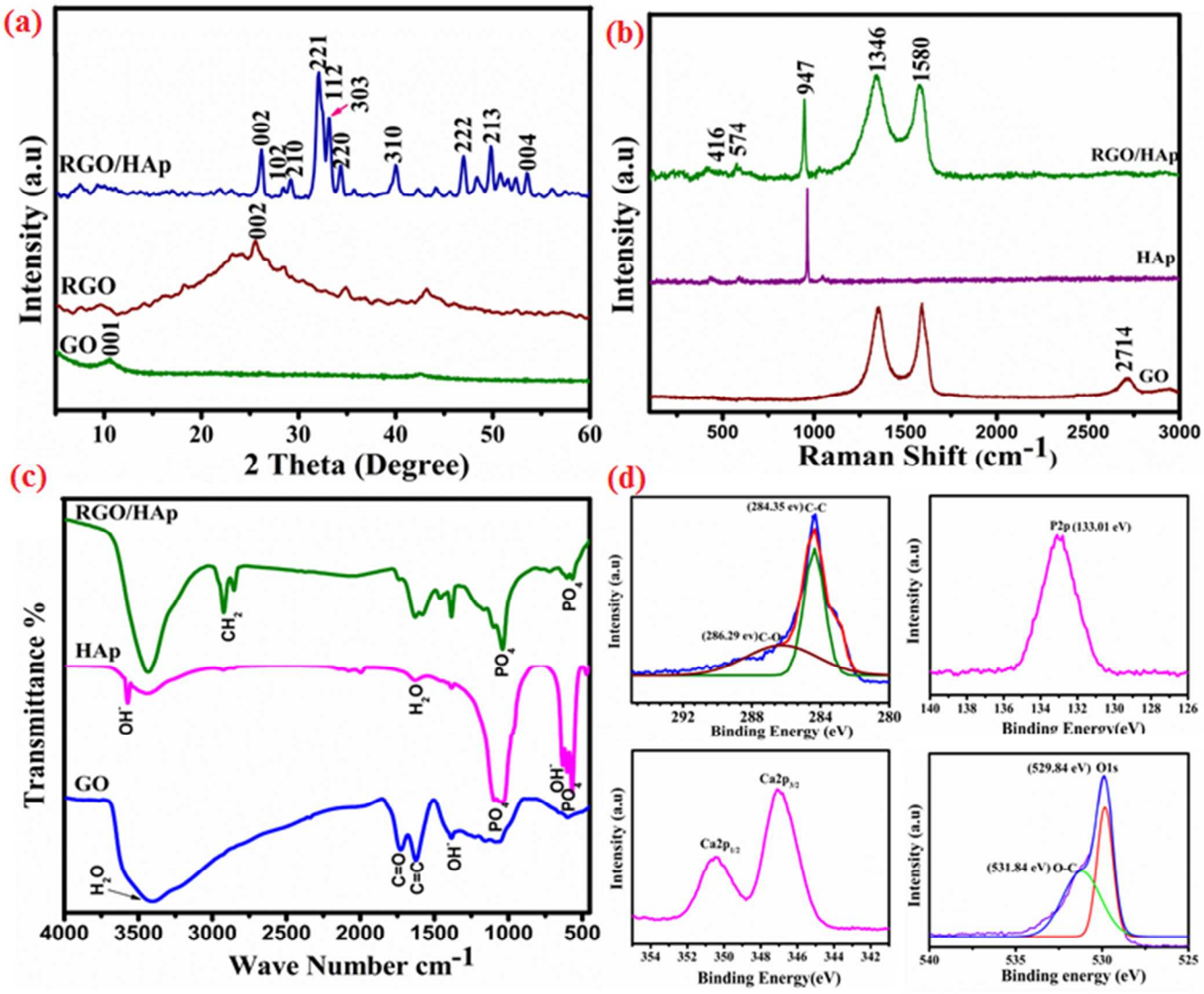

Fig. 3 (a-c) X-ray powder diffraction pattern, Raman spectra and FTIR spectra of G0, RGO and RGO/Hap, (d) XPS high resolution spectra of RGO/HAp nanocomposite Ca2p, P2p, C1s and O1s.

Furthermore, the UV-vis spectroscopy can be used to find the chemical structure of the GO and RGO.[22] Fig. S1 shows the three types of characteristic features. The peak at 230 nm was due to π- π* plasmon peak for the nanoscale sp^2 C=C aromatic transition bonds. The other peak at 310 nm was attributed to n-π* transition peak of sp^3C=O bonds and a shoulder at 267 nm was due to the red shift of GO to RGO for the RGO/HAp nanocomposite during the hydrothermal reaction. Furthermore, Fig. S2 displays the UV-vis spectrum of GOx, which shows the two well-defined absorption peaks at 380 and 455 nm reveals the presence of oxidized form of FAD group in GOx. After immobilizing GOx on RGO/HAp 50 consecutive cycles were recorded at pH 7 and the electrode was sonicated in 2 ml of pH 7 PBS and UV-vis absorption spectra were recorded. Similar to the absorption band of native GOx, the immobilized GOx exhibits the same characteristic band, showing that GOx

immobilized on the RGO/HAp retain its native structure without denaturation.[23]

3.2 Nucleation and Growth Mechanism

The growth mechanism of the RGO/HAp (1D on 2D structure) nanocomposite was proposed based on the observed experimental results. Scheme 1 shows the schematic illustration for the formation of HAp nanorods on the RGO sheets. The graphite oxide was prepared by modified Hummer's method with a higher degree of oxidation of natural graphite flaks.[22] Subsequently, C:O ratio was increased to form oxygen containing groups such as carbonyl and carboxyl groups. These groups were located at the edges and more number of the hydroxyl and epoxy group at the basal plane of graphene sheets.

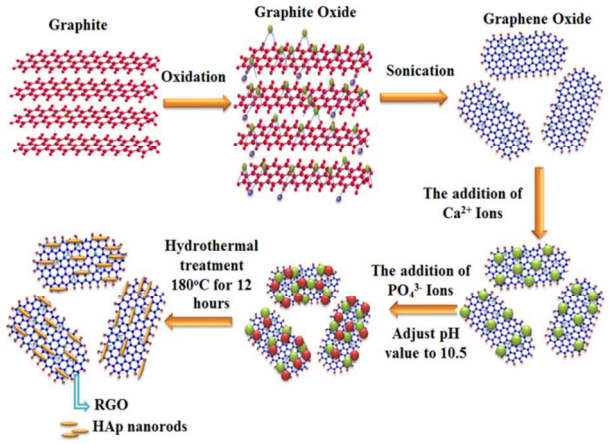

Scheme 1 Schematic illustrations for the formation mechanism of 1D HAp on 2D RGO sheets.

Thus, the graphite oxide can be exfoliated under sonication to form a highly stable, brown colour suspension in water. Those oxygen containing groups was possibly involved in the formation of HAp nanorods anchored on the surface of negatively charged graphene oxide sheets. Then, certain concentration of $CaCl_2.2H_2O$ was added to the graphene oxide solution, the Ca^{2+} was selectively bonded with epoxy, hydroxyl and carboxyl group through electrostatic interactions.[20,24] The Ca^{2+} ions approaching the surface of a graphene oxide with hydroxyl (HO-Graphene oxide), epoxy (EO-Graphene oxide) and carboxyl (HO-O-Graphene oxide) functional groups. The Ca^{2+} ions easily diffuse and prefer the crystallization and growth of HAp nuclei on the basal planes as well as edges of the graphene oxide sheets. Further, the Ca^{2+} ions react with phosphate (PO_4^{3-}) ions via electrovalent bonds on adjusting the pH. Finally the HAp nuclei were formed on the basal planes and edges of the RGO sheets along *c-axis* which were confirmed through FESEM images. In general, the hydrothermal reduction at high temperature was reported to be a unique route to repair aromatic sp^2 hybridized network during the post reduction.[25] As a result, the GO was reduced to form RGO, escorted with the growth of 1D HAp nanorods on the 2D RGO support during the hydrothermal reaction.

3.3 Direct electrochemistry of glucose oxidase (GOx)-1D HAp-on-2D RGO modified electrodes

Cyclic voltammetry (CV) is an important technique to study the direct electrochemisty of GOx on the 1D HAp-on-2D RGO nanomaterials. Glucose oxidase (GOx) was taken as a typical enzyme to explore the application of 1D HAp-on-2D RGO nanostructures for biosensing due to their prominent role in glucose monitoring. The direct electrochemistry of GOx immobilized 1D HAp on 2D RGO modified electrode was examined in N_2 saturated PBS (pH 7) with the scan rate of 50 mV s^{-1}. Fig. 4a shows the cyclic voltammograms of GOx (curve d'), Hap/GOx (curve c'), RGO/GOx (curve b') and RGO/Hap/GOx (curve a') modified GCEs in PBS (pH 7) at a scan rate of 50 mV s^{-1}. The curve d' corresponds to the electrochemical signal of the GOx/GCE which shows a featureless redox peaks within the potential range of -0.9 to 0.5 V. Curve b' and c' represents the immobilized GOx in RGO and HAp giving a pair of redox peaks with negligible redox peak current. Furthermore, a pair of well-defined and quasi-reversible redox peaks with a peak to peak separation of 60 mV (ΔEp) at 50 mVs^{-1} was observed as shown in for the RGO/HAp/GOx modified GCE (curve a'). In comparison, the CV curve for RGO/HAp/GOx modified GCE is apparently larger than the pure HAp and RGO nanoparticles. Meanwhile, the highly mesoporous RGO/HAp/GOx modified GCE shows a well-defined redox peak, which designates the favorable direct electron transfer of GOx on the electrode. This redox peak is ascribed to the electrochemical reduction reaction of FAD. The anodic peak current (I_{pa}) at -0.3 V relates to the conversion of FAD to $FADH_2$ and the cathodic peak current (I_{pc}) at -0.4 V corresponds to the conversion of $FADH_2$ to FAD. This strongly confirms that the direct electrochemical reaction of GOx occurs

on the surface of mesoporous RGO/HAp/GOx electrode. The result suggests that the GOx retain their bioactivity on the mesoporous RGO/HAp/GOx surface. The direct electron transfer of Glucose Oxidase (GOx) is a two electron ($2e^-$) along with two-proton ($2H^+$) reaction process and the reaction mechanisms are shown in Eqn. 1.

$$GOx/FAD + 2e^- + 2H^+ \leftrightarrow GOx/FADH_2 \quad (1)$$

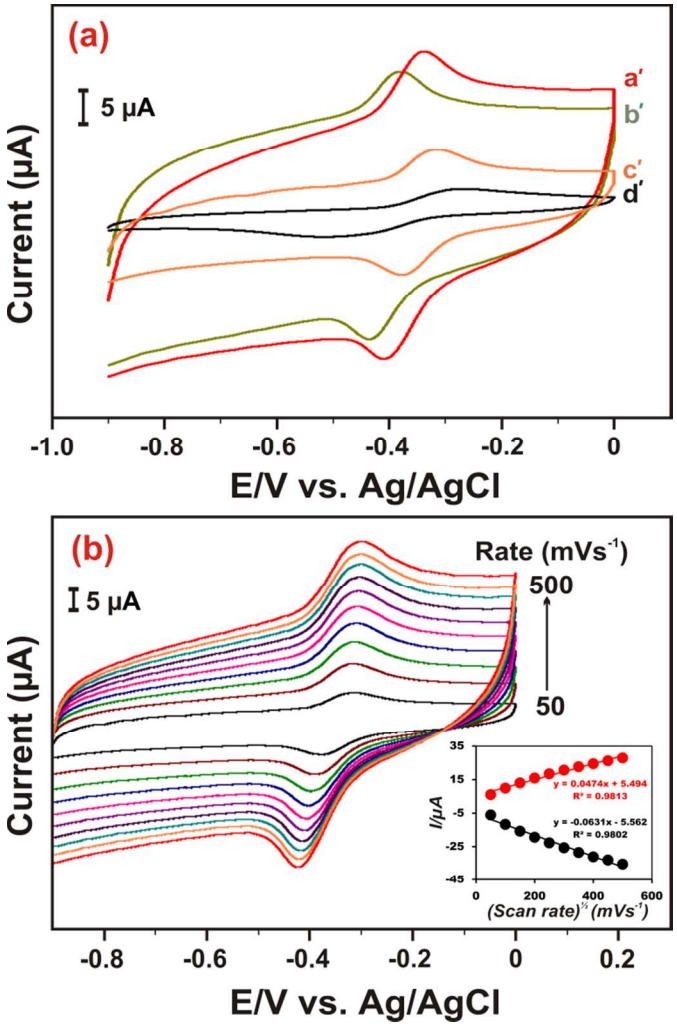

Fig. 4 (a) Cyclic voltammogram of (a) RGO/HAp/GOx, (b) RGO/GOx, HAp/GOx (c) and (d) GCE/GOx modified GCE in N_2 saturated PBS (pH 7) at a scan rate of 50 mV s^{-1}. (b) Cyclic voltammograms of RGO/HAp/GOx modified GCE in deoxygenated PBS at different scan rates (50-500 mVs^{-1}). Inset in Fig (b) shows the linear dependence of peak currents with scan rate.

3.4 Effect of scan rate and pH

The cyclic voltammograms with different scan rates are also measured and shown in Fig. 4b for the RGO/HAp/GOx modified electrode in N_2 saturated PBS. The oxidative and reductive peak current increases instantaneously together with the enlarged peak to peak separation with the increase of scan rate from 50 to 500 mVs^{-1}. Further, a small peak shift was observed in both anodic and cathodic peak current. The linear dependence of anodic peak current (I_{pa}) and cathodic peak current (I_{pc}) on scan rate is given in the inset of Fig. 4b, suggesting a surface-controlled quasi-reversible process. The linear regression equations for the I_{pa} is 0.0474x+5.494; R^2=0.9813 and I_{pc} is -0.0631x+(-5.562); R^2=0.9802, where, x is the scan rate. From the integration of the reduction peaks of the mesoporous RGO/HAp/GOx at 500 mVs^{-1}, the surface coverage of GOx can be calculated to be 3.48×10^{-10} mol cm^{-2} which was higher than the reported values.[26,27]

This result proves that the large specific area of RGO/HAp nanocomposites facilitate the high enzyme loading capacity. The electron rate constant (K_s) can be calculated by using the Laviron Equation[28] at a high scan rate (500 mVs^{-1}) from CV measurements ($n\Delta E_p > 0.200$ V)

$$\log K_S = \alpha\log(1-\alpha) + (1-\alpha)\log\alpha - \log(RT/nF\nu) - \alpha(1-\alpha)nF\Delta E_p/2.3RT \quad (2)$$

Where α is the charge transfer coefficient (~0.5) and other parameters signifying their usual meanings. The K_s value for the RGO/HAp/GOx film modified GCE has been calculated as 3.50 s^{-1}, which was relatively larger than that observed for GOx immobilized on MWCNT (1.53 s^{-1}), boron doped CNT (1.56 s^{-1}), SWCNT (0. 3s^{-1}), graphene/chitosan (2.83 s^{-1}), and P-taurine/GOx/nf (1.38 s^{-1}) modified electrodes.[26,27,29] Hence, this larger rate constant of RGO/HAp/GOx modified GCE facilitate the fast electron transfer between glucose oxidase (GOx) and electrode surface.

The pH is an effective parameter for GOx to preserve their activity and catalytic proficiency. Fig. 5 shows the cyclic voltammograms of RGO/HAp/GOx modified GCE with the range of pH from 1 to 11. The following equation represents the direct electrochemistry of glucose oxidase (GOx) on the modified electrode depicting a two proton ($2H^+$) redox reaction process.[30] It has assumed that the concentrations (C) of GOx/FAD and GOx/$FADH_2$ were constant during the change in the pH value of the solutions. Accordingly, the peak potential of reversible redox electrochemical mechanism is shown in Eqn.1.[20,31]

$$E = E^0 + \frac{2.3RT}{nF}\log\left[C_{GOx/FAD} \times (C_{H^+})^2 / C_{GOx/FADH_2}\right] \quad (3)$$

$$E = E^0 - \frac{2.3RT \times 2}{nF} pH \quad (4)$$

$$E^0 = cons\tan t + 0.059\, pH \quad (5)$$

Where R, T, n and F are the gas constant, temperature, number of the electron transfer involved and Faraday constant respectively.

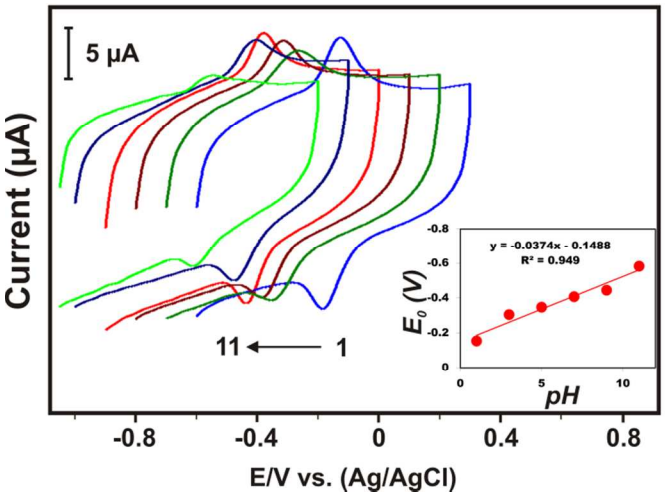

Fig. 5 Cyclic voltammograms obtained for RGO/HAp/GOx composite film modified GCE in deoxygenated buffer solutions by varying the pH from 1 to 11 with the scan rate of 50 mVs^{-1}.

The theoretical value of the slope of formal potential E^0 versus pH must be 57 mV/pH. The change in the pH influences the cathodic (I_{pc}) and anodic (I_{pa}) peak currents and formal potential (E^0). The formal potential was shifted towards negative by increasing the pH value of the solutions. The increase in the pH increases the anodic and cathodic peak currents and also it reaches a maximum at the pH of 7. The peak current gradually decreases with the increase of pH due to the decrease of proton ($2H^+$) concentration and bioactivity of the immobilized glucose oxidase (GOx). The inset in Fig. 5 shows the linear variation of formal potential (E^0) by different pH values and the slope is -57/pH (0.949) and it was close to the theoretically predicted value of -59/pH. Therefore, the direct electrochemical reaction of GOx on the RGO/HAp modified GCE is a two proton ($2H^+$) coupled with two electron ($2e^-$) reversible redox process.

Based on the pH solution, HAp possesses both positive and negative surface charge, which provides multiple adsorbing sites. The isoelectric point of glucose oxidase is 4.2. Acidic proteins bind to HAp through the carboxyl groups. Due to the electrostatic repulsion between the carboxyl groups and the negatively charged sites, the COOH groups bind specifically to the Ca^{2+} sites of HAp.[17] Therefore, GOx was immobilized on HAp through electrostatic interactions. After immobilizing GOx on RGO/HAp 50 consecutive cycles were recorded in pH 7 and the electrode was sonicated in 2 mL of pH 7 PBS and UV-vis absorption spectra (Fig. S2) were recorded. Similar to the absorption band of native GOx, the immobilized GOx exhibits two well-defined absorption peaks at 380 and 455 nm, showing that GOx immobilized on the RGO/HAp retains its native structure without denaturation.

3.5 Electrocatalytic activities and biosensors application of RGO/HAp/GOx modified electrode

The fast direct electron transfer rate, admirable GOx immobilization capacity and negative redox potential of -0.45 V of the RGO/HAp nanocomposite offer a significant improvement to construct a novel biosensor. Since most of the biosensors depends on the indirect electrochemistry and frequently requires higher oxidation potentials.

Thus, the peak current measurement suffers considerably from the interference of the oxidation of uric acid (UA), dopamine (DA) and ascorbic acid (AA) etc., which present in the biological fluids. A negative redox potential (-0.45 V) of the direct electrochemistry on the RGO/Hap nanocomposites has an effective electrocatalytic activity and significantly reduces the interference of the oxidation. In contrast, the electrochemical detection of glucose was indirectly realized by monitoring the oxygen consumption by the enzyme-catalyzed reaction process as explained below. Fig. 6a shows the CVs of RGO/HAp/GOx modified GCE in N_2 and O_2 saturated 0.01 mM PBS with a scan rate of 50 m V s^{-1}. A couple of well-defined redox peak currents are observed in both N_2 and O_2 saturated PBS. In the presence of oxygen, the conversion of $GOx/FADH_2$ was further oxidized by dissolved oxygen at the surface of electrodes generating hydrogen peroxide (H_2O_2)

$$GOx/FADH_2 + O_2 \rightarrow GOx/FAD + H_2O_2 \quad (6)$$

As evidenced from Fig. 6a, the cathodic peak current is larger than the anodic peak current in the O_2 saturated PBS as

compared with the reliable peak current in the N_2 saturated PBS. Fig. 6b shows the CVs of RGO/HAp/GOx modified GCE biosensor in the presence of various concentrations of glucose (0 to 39.2 mM) in O_2 saturated PBS at a fixed potential with the scan rate of 50 mV s^{-1}. It shows the decrease in the cathodic peak current (Ip_c) with the linear increase of glucose concentration (a-k) due to the consumption of dissolved oxygen. This confirms the RGO/HAp/GOx modified GCE possess higher electrocatalytic activity for the glucose sensor. Therefore, the cathodic peak current and glucose concentration are linearly proportional with the correlation coefficient of R^2=0.9506.

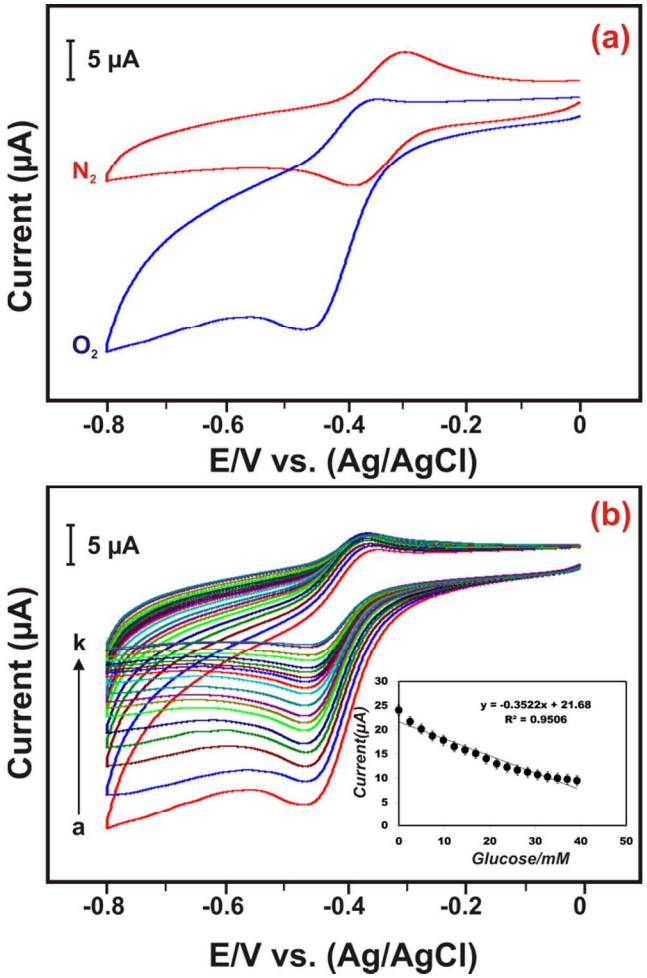

Fig. 6 (a) Comparison of CV catalase of N_2 and O_2 saturated PBS of RGO/HAp/GOx hybrid bio nanocomposite modified electrode in the presence of 0.1 mM glucose with the scan rate of 50 mV s^{-1} and (b) Cyclic voltammograms of RGO/HAp/GOx modified electrode for the addition of 0- 39.2 mM glucose (a-k) in oxygen saturated PBS with the scan rate of 50 mV s^{-1}. Inset in Fig. (b) Shows the linear dependence of peak currents *vs* concentration of glucose.

3.6 Sensing Mechanism

Schematic 2 describes the sensing mechanism for the proposed glucose biosensors based on RGO/HAp/GOx nanocomposite modified GCEs. The GOx can act as a catalyst and it was adsorbed on the surface of RGO/HAp nanorods by the simple drop casting process. The adsorption ability of GOx depends on the specific surface area (SSA) and surface charge of 1D HAp on 2D RGO nanosheets. The RGO/HAp exhibits high specific surface area, uniform pore size distributions and different kinds of surface charges. The surface charge of HAp nanocrystals eventually depends on the competing growth of *a*, *b* and *c*-surface planes.[31,32] The XRD and FESEM results confirm the growth of 1D HAp on 2D RGO.

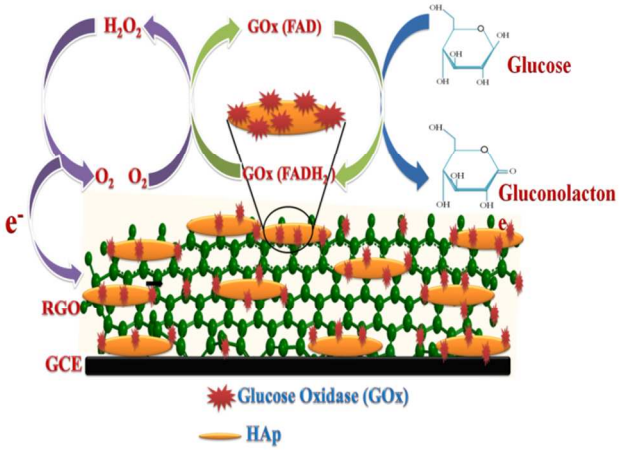

Scheme 2 Schematic illustration for the mechanism of glucose sensing based on RGO/HAp/GOx nanocomposite.

The HAp primitive cell *c*-axis (001) surface contains one Ca^{2+} ions and 4/4 hydroxyl groups and therefore positively charged calcium is rich on the basal plane (*c*- surface). In contrast, the prismatic plane (*a*-surface) is hydroxyl and phosphate rich, and hence negatively charged.[31,16] Thus, the HAp nanorods have rich Ca^{2+} ions resulting negatively charged GOx are electrostatically attracted with positively charged *c*-surface and enhances more adsorption binding ability of GOx on HAp surfaces. The GOx could be immobilized on RGO/HAp due to their ultrafine size, omnidirectional contacts to the surface and positively shorten the electron tunnelling between the GOx active centres and RGO/HAp conductive electrode surface. The oxidation of glucose in the presence of GOx can be occurred during the glucose sensing for the following two processes. Initially the reduction of flavin group (FAD) in the GOx reacting with glucose provides the reduced

form of GOx ($FADH_2$) as shown in Eqn.1. Further the GOx/$FADH_2$ was oxidized due to dissolved oxygen to regenerate the oxidized form of the GOx (FAD) and H_2O_2 during the enzymatic reaction of GOx and D-glucose at the conductive RGO/HAp surface and it could generate a redox current as shown in Eqn.1 and Eqn.7. The quantification of glucose can be realized through electrochemical detection of enzymatically liberated H_2O_2:

$$H_2O_2 \rightarrow O_2 + 2H^+ + 2e^- \quad (7)$$

The characteristic redox peak current was higher on RGO/HAp/GOx nanocomposite modified electrode. It also exhibits the excellent reversible electron transfer redox behavior at -0.4 V. It reveals the synergistic effect of RGO/HAp/GOx, which plays a key role to facilitate the direct electron transfer between GOx and the electrode surface results the enhanced detection of glucose.

3.7 Amperometric Determination of Glucose at RGO/HAp/GOx Modified Electrode

The amperometric glucose determination was performed under optimized conditions with rotating disc electrode (RDE). The work functions of the electrodes are based on Bard and Faulkner experimental procedure.[33] This hydrodynamic electrochemical method comprises the convective mass transport of reactants and products at the surface of the electrode when it is rotated at a specific speed of 1500 rpm. Fig. S3a shows the electrochemical biosensing of glucose recognized with amperometric response of modified RDE with RGO/HAp electrode immobilized with GOx with an applied potential of -0.43 V in oxygen saturated PBS. The performance of this amperometric glucose biosensors based on the observation of amperometric responses generated by oxygen reduction upon the increase of glucose concentrations to the solutions. The reaction vessel was properly covered during the detection of amperometric response of glucose to maintain the oxygen atmosphere above the experimental solutions. The oxygen content of the solution gradually decreases with the addition of glucose at regular intervals of time (50 s). Small peaks were instantly observed for the successive addition of minimum concentration of glucose (0.1-1.6 mM) as shown in Fig. S3a, and these peaks represents the reduction of oxygen. A further increase in the glucose concentration as well as oxygen consumption resulting a gradual decrease in the voltammetric current and finally levels off with the higher concentration of glucose (19.82 mM). The oxygen (O_2) consumption relatively increases with the addition of glucose in each time to the solution resulting in a decrease of catalytic current. However, we observed a slight decrease in the background, current without adding glucose may likely be due to the loss of surface active sites as a result of adsorption of intermediate species on the catalyst surface also been reported at other GOx modified electrodes.[33-35] The inset in Fig. S3a shows the linear dependence of the peak (catalytic) current with glucose concentration. The result shows that the RGO/HAp nanocomposite modified RDE has a steady state amperometry response in the range of 0.1 to 19.2 mM of glucose with the correlation coefficient of 0.9852. The sensitivity and detection limit of the biosensor is 16.9 μA mM^{-1} cm^{-2} and 0.03 mM which is higher than that of other reported electrodes as shown in Table 1.

3.8 Selectivity, Stability, Reproducibility of the Biosensor

The selectivity of the RGO/HAp/GOx modified GCE was evaluated in the presence of common interfering species such as dopamine, uric acid and ascorbic acid in oxygenated PBS. Fig. S3b shows the amperometric response of the RGO/HAp/GOx modified GCE with the successive addition of 0.05 mM glucose. The fabricated biosensor has a rapid response with every addition of glucose. However, no significant response was observed for the addition of 0.5 mM of dopamine, 0.2 mM of uric acid, 0.2 mM of ascorbic acid and 0.2 mM of L-cysteine. Thus, the RGO/HAp/GOx film is highly selective for the detection of glucose and it can be applied for glucose determination in real sample analysis. The stability of the fabricated biosensor was investigated by storing the RGO/HAp/GOx modified GCE in PBS (pH 7) at 4°C and the current response was observed periodically by using CV. After 25 days the biosensor retains the stability of 89.4% reveals its good stability and could be attributed to the good sensing capability of the RGO/HAp with the effective immobilization of GOx. The reproducibility was investigated by fabricating three individual electrodes of RGO/HAp/GOx and studied their responses to 0.05 mM glucose in O_2 saturated PBS and measured under identical conditions. The relative standard

deviation (RSD) of the response was 3.69%, which indicates the fabricated electrode exhibits appreciable reproducibility.

3.9 Determination of glucose in various urine samples

In order to prove the real time application of the reported biosensor, urine samples were collected from diabetes patient and healthy man have been employed for real sample analysis. The results are shown in Table S1 and the obtained recoveries ranged between 96.3% and 103.6%. The significant recoveries achieved in various urine samples for the determination of glucose reveals the practicality of the biosensor.

4. Conclusions

In summary, the 1D HAp nanorods were uniformly grown on 2D RGO by a novel hydrothermal process. The hydrothermal reaction temperature promotes the crystallinity of HAp with the simultaneous reduction of GO to RGO. The GOx immobilized RGO/HAp nanocomposite modified GCE electrodes demonstrates the direct electrochemical detection of glucose. The glucose sensing mechanism of GOx immobilized on RGO/HAp nanocomposite was verified by cyclic voltammetry (CV) in both O_2 and N_2 saturated PBS. The obtained result confirms the glucose oxidation by GOx resulting in significant decrease of cathodic peak current (I_{pc}) and it can be used for high sensitive glucose detection. The amperometric glucose sensing shows the modified GCE electrodes have a wide linear amperometric response with the sensitivity and detection limit of 16.9 μA mM^{-1} cm^{-2} and 0.03 mM respectively. The obtained results confirm the fabricated electrode is more suitable for the development of enzyme based biosensors.

Acknowledgements

The authors greatly acknowledge the University Grant Commission (UGC), New Delhi, Government of India for the financial support and DST-FIST, Government of India for FESEM facility.

References

1 Joseph Wang, *Chem. Rev*., 2008, **108**, 814−825.
2 C. Fu, W. Yang, X. Chen, D. G. Evans, *Electrochem. Commun.,* 2009, **11**, 997–1000.
3 L. Hua, X.Wu and R.Wang, *Analyst*, 2012, **137**, 5716–5719.
4 Y. Guo, Y. Han, S. Shuang and C. Dong, *J. Mater. Chem*., 2012, **22**, 13166–13173.
5 S.J. Bao, C. M. Li, J. F. Zang, X. Q. Cui, Y. Qiao,and J. Guo, *Adv. Funct. Mater*, 2008, **18**, 591–599.
6 S.S. Ray, and M. Okamoto, *Prog.Polym. Sci.* 2003, **28**, 1539-1641.
7 X. Huo, J. Liu, B. Wang, H. Zhang, Z. Yang, X. She and P. Xi, *J. Mater. Chem.A*, 2013, **1**, 651.
8 L. J. Bonderer, A. R. Studart, and L. J. Gauckler, *Science*, 2008, **319**, 1069-1073.
9 Ying, W., Yuyan, S., Dean, W.M., Jinghong, L., Yuehe, L., 2010. ACS Nano 4, 1790-1798.
10 A. Zangwill, and D.D. Vvedensky, *NanoLett*. 2011, **11**, 2092–2095.
11 H. K. Kim, C. Mattevi, M. R. Calvo, J. C. Oberg, L. Artiglia, S. Agnoli, C. F. Hirjibehedin, M. Chhowalla, and E. Saiz, *ACS Nano*, 2012, **6**, 3614-3623.
12 X. Huo, J. Liu, B. Wang, H. Zhang, Z. Yang, X. She and P. Xi, *J. Mater. Chem.A*, 2013, **1**, 651.
13 Y. Ma, M. Zhao, B. Cai, W. Wang, Z.Ye and J. Huang, *Biosens. Bioelectron*, 2014, ***59***, 384-388.
14 Y. Ma, M. Zhao, B. Cai, W. Wang, Z. Ye and J. Huang, *Chem. Commun*.,2014, ***50***, 11135-11138.
15 J.C. Claussen, A. D. Franklin, A. Haque, D. M. Porterfield, and T. S. Fisher, *ACS Nano*, 2009, **3**, 37-44.
16 G. Bharath, A. Jagadeesh Kumar, K. Karthick, D. Mangalaraj, C. Viswanathan and N. Ponpandian, *RSC Adv*., 2014, **4**, 37446-37457.
17 M.R. Na, W. Bin, L. Yan, L. Jing, Z. Qian, W. G.Tao, J. W. Li and W. H. Sheng, *Sci China Ser B-Chem*. 2009, **52**, 2013-2019.
18 J. Li, D. Kuang, Y. Feng, F. Zhang and M. Liu, *MicrochimActa*, 2012,**176**,73–80.
19 M. Zhao, J. Huang, Y. Zhou, Q. Chen, X. Pan, H. He, Z.Ye, *Biosens. Bioelectron*, 2013, ***43***, 226-230.
20 M. Li, Y. Wang, Q. Liu, Q. Li, Y. Cheng, Y. Zheng, T. Xi and S. Wei, *J. Mater. Chem. B*, 2013, **1**, 475- 484.
21 W. S. Hummers, and R. E. Offeman, *J. Am. Chem. Soc.,* 1958, **80** , 1339-1339.
22 Q. Lai, S. Zhu, X. Luo, M. Zou, and S. Huang, *AIP Advances*, 2012, **2**, 032146-(1-5).
23 A.T. Ezhil Vilian, Shen-Ming Chen, M. Ajmal Ali and F.M.A. Al-Hemaid, RSC Adv., 2014, **4,** 30358-30367.
24 S. Baradaran, E. Moghaddam, W.J. Basirun , M. Mehrali , M. Sookhakian, M. Hamdif, M.R. Nakhaei Moghaddam and Y. Alias, *Carbon*, 2014, **69**, 32–45.
25 C. B. Navarro, E. Coronado, C. M. Gastaldo, J. F. Sa'nchez-Royo and M Go'mez, ***Nanoscale*****,** 2012, **4**, 3977-3982.
26 C. X. Cai, J. Chen, Anal. Biochem.2004, 332, 75.
27 C. Deng, J. Chen, X. Chen, C. Xiao, L. Nie, S. Yao, Biosens. Bioelectron., 2008, 23, 1272-1277.
28 E. Laviron, E., J. Electroanal. Chem,1979, **101**, 19-28.
29 Madhu, R., Devadas, B., Chen, S-M., Rajkumar, M., 2014. *Anal. Methods***,** 2014,**6**, 9053-9058.
30 P. Wang, Y. Zhai, D. Wang and S. Dong, *Nanoscale*, 2011, **3**, 1640-1645.
31 A. J. Bard, L. R. Faulkner, Electrochemical Methods, 2nd ed., John Wiley & Sons, Inc, New York 2001, p. 228–242.
32 J. Q. Liu, A. Chou, W. Rahmat, Electroanal. 2005, 17, 38.
33 B. Unnikrishnan, S. Palanisamy, S-M. Chen, Biosens. *Bioelectron.*, 2013, **39**, 70-75.
34 C. Xu, Y. Liu, J. Wang, H. Geng and H. Qiu, J. Power Sources, 2012, 199, 124–131.
35 A.P. Periasamy J. Mater. Chem. A, 2014, 2, 11899–11904.
36 M.A. Rong, W. Bin, L. Yan, L. Jing, Z. Qian, W. G. Tao, J. WenLi and W. H. Sheng, *Sci China Ser B-Chem*., 2009, **52**, 2013-2019.

37 Z. Wang, X. Zhou, J. Zhang, F. Boey and H. Zhang, *J. Phys. Chem. C*, 2009, **113**,14071-14075.
38 J. Lu, L. T. Drzal, R. M. Worden and I. Le, *Chem. Mater*., 2007, **19**, 6240–6246.
39 S. Liu, J. Tian, L. Wang, Y. Luo, W. Lu, X. Sun, *Biosens. Bioelectron*., 2011, **26**, 4491-4496.
40 Y. Liu, D. Yu, C. Zeng, Z. Miao and L. Dai, *Langmuir*, 2010, **26**, 6158-616.

Table 1: Comparison of analytical parameters for detection of glucose over various modified electrodes

Glassy carbon modified electrode	Limit of detection (mM)	Linear response range (mM)	Sensitivity	Techniques	Ref.
HAp[a]-GOx[b]- Nafion	0.02	0.12-2.16	6.75 mA M^{-1}	Amperometric	33
RGO[c]-GOx	-	0.1-27	1.85 µA mM^{-1} cm^{-2}	Amperometric	34
APTES[d]-rGO-GOx	-	1-24	-	CV[e]	35
GNSs[f] -GOx-Nafion	-	0.2-1.4	3.4 µA mM^{-1}	CV	2
xGnP[g]-GOx-Nafion	0.01	1-6	14.17 µA mM^{-1} cm^{-2}	Amperometric	38
GP[h]-GOx	0.02	2-22	-	CV	39
RGO-GOx	-	1-22	8.045 mA M^{-1} cm^{-2}	Amperometric	40
RGO[c]/HAp[a]/GOx	0.03	0.1-11.5	16.9 µA/$mM^{-1}$$cm^{-2}$	Amperometric	**This work**

[a]a-hydroxyapatite, b-glucose oxidase, c-reduced graphene oxide, d-3-aminopropyltriethoxysilane, e-Cyclic Voltammetry, f-exfoliated graphite nanosheet, g-Exfoliated graphite nanoplatelets, h-Graphene platelet, i-Electrochemically reduced graphene oxide, j-Multi walled carbon nanotube

Title of the content

Enzymatic Electrochemical Glucose Biosensors by Mesoporous 1D Hydroxyapatite on 2D Reduced Graphene Oxide

G. Bharath,[a] R. Madhu,[b] Shen-Ming Chen,[b] V. Veeramani,[b] A. Balamurugan,[a] D. Mangalaraj,[a] C. Viswanathan,[a] N. Ponpandian*[,a]

A hydrothermal synthesized mesoporous 1D HAp on 2D RGO sheets exhibiting direct electrochemistry of glucose bio sensing.